Revisiting the redox transitions of Polyaniline. Semiquantitative interpretation of electrochemically induced IR bands

F. Huerta [a], C. Quijada [a], F. Montilla [b],*, E. Morallón [b]

[a] Departamento de Ingenieria Textil y Papelera, Universitat Politecnica de Valencia, Plaza Ferrandiz y Carbonell, 1, Alcoy E-03801, Spain
[b] Departamento de Química Física e Instituto Universitario de Materiales de Alicante. Universidad de Alicante. Crtra. San Vicente s/n, Alicante E-03690, Spain

A R T I C L E   I N F O

A B S T R A C T

The redox transitions of PANI in acidic medium have been monitored by a combination of cyclic voltammetry, *in situ* conductance and *in situ* FTIR spectroscopy. The results of the semiquantitative analysis strongly suggest that the classical tetrameric model of PANI does not satisfactorily describe the actual structures of the polymer at different redox states. An octameric model is revisited, with the inclusion of essential resonant structures, to provide an appropriate prediction of the relative IR intensity changes of the aromatic C—C stretching (at around 1520 cm^{-1}) and the quinoid C=C stretching (at around 1590 cm^{-1}) vibrations observed by FTIR, which are difficult to interpret by considering only 4 aniline rings. Particularly, it is found that the emeraldine state is better described as a resonance hybrid of the classical bipolaronic and semiquinoid (polaron lattice) structures, while most of the charge transferred at the onset of the second voltammetric peak comes from the additional oxidation of this hybrid, which becomes unstable in the electrochemical environment producing mineralization to CO_2 and release of soluble quinones.

1. Introduction

Polymers containing non-localized electrons in their backbones are often referred to as conducting polymers. A great deal of both scientific and technological interest has been devoted to the fundamental electrochemistry of these systems owing to their dual character. On the one hand, they show semiconducting properties in the native (un-doped) state that allow its use as replacement of inorganic semiconductors in, essentially, all the existing electronic devices: transistors, diodes, solar cells, etc. giving rise to a new scientific-technological field called organic (or plastic) electronics [1]. On the other hand, the progressive oxidation (or reduction) of the polymer backbone (doping process) increases the conductivity of the material by several orders of magnitude. This behavior, and additional physicochemical properties, supported their applicability to non-linear optics, electrocatalysis, electrochemomechanical devices or charge storage systems, among other research fields [2].

The electrochemical oxidation of resonant aromatic molecules such as pyrrole, thiophene, aniline and their derivatives has become one of the main methods used to prepare conjugated, electronically conducting polymers [3,4]. Polyaniline (PANI) and its derivatives are probably the most studied conducting polymers synthesized by electrochemical methods [5–8]. Even before the advent of macromolecular chemistry,

the existence of polyaniline (known initially as aniline-black) was recognized although the concept of polymer itself did not exist [9]. The first studies on aniline-black come from the 19th century [10] but it was in the early 20th century that the works of Willstatter, Moore, Green and Woodhead defined the different oxidation states of an eight-unit molecule (the so-called eight-nucleal structure, since the term oligomer was not defined yet) considered precursors of aniline-black [11,12]. Already at that time the complex redox structure of aniline-black was recognized and the terminology related to the different oxidation states of the octamer was assigned, the so-called leucoemeraldine, protoemeraldine, emeraldine, nigraniline and pernigraniline. These states correspond to 0, 25, 50, 75 and 100% of oxidized rings, respectively [12]. Once the polymeric character of PANI was identified after the first quarter of the 20th century, this compound went quite unnoticed until its rediscovery as a conducting polymer in the mid-1980s. In this sense, MacDiarmid's seminal papers led to establishing that PANI presents a conductivity influenced by the pH of the synthesis medium and demonstrated that the conductive forms of PANI only appear at pH lower than 4 [13].

The redox species that provides electric conductivity to this polymer is the protonated emeraldine, which suffers an internal redox reaction giving rise to a semiquinone or separate polaron radical-cation [14–16], Scheme 1. From an electrochemical point-of-view,

PANI adopts its fully reduced state (leucoemeraldine) at cathodic potentials and, as the applied potential is made more positive, the polymer backbone gradually oxidizes to emeraldine (the intermediate oxidation state) and, subsequently, to pernigraniline (the fully oxidized state). The electrochemical oxidation of the reduced form of PANI results in anion inclusion to maintain the electro-neutrality [5,7].

The three oxidation states referred above may be protonated or not, although the fully reduced form may not contain significant amounts of protonated units, even at very low pH. Some studies showed counter-anions being expelled out of the film during the electrochemical reduction of PANI [17–19]. The emeraldine state presents two isoelectronic resonant configurations with polaronic and bipolaronic structures [20]. This oxidation state is the unique electron-conducting form of PANI and the charge transport occurs via a hopping mechanism, where the electronic states remain localized [21]. It is generally accepted that conduction implies the interchange of reduced (benzenoid) and oxidized (quinoid) domains via a tautomeric proton migration between nitrogen atoms [22]. The fully oxidized polymer (pernigraniline) seems to release counter-anions and hence to be unprotonated, which results in a substantial decrease in electronic conductivity [23,24]

A variety of experimental techniques have been applied traditionally to characterize PANI, including elemental analysis, electrochemical methods, microscopy techniques and *ex-situ* spectroscopies such as FTIR, Raman or XPS that are powerful tools to characterize the polymer at a molecular level. In contrast to the *ex-situ*, the use of *in situ* techniques ensures the integrity of the film during the analysis and, besides, allows the inspection of the film under potential control. In this way, one can obtain direct information on the film condition at every potential and follow the molecular changes related to variations on the redox state of the polymer. Some *in situ* techniques applied to the characterization of PANI were Raman spectroscopy [25], UV–visible spectroscopy [26–28] or conductimetry studies [29–33], among others [34,35]. Particularly, *in situ* FTIR spectroscopy is recognized as a key tool to follow the polymerization process of PANI [36], determine its molecular structure as a function of the potential [19,37,38] and confirm degradation pathways [39]. However, to the best of our knowledge, none of the above techniques have been used to provide a deep quantitative characterization of the various chemical structures/species that prevail at the different oxidation states/doping levels. The present contribution aims to provide a novel semiquantitative model based on a combination of *in situ* FTIR and conductance measurements. The overoxidation process will be also investigated. Semi-quantitative information will be extracted from the integration

of IR absorption bands, which will be correlated with the doping level of the polymer. The approach will provide deeper knowledge on the true nature of the species involved in the redox transformations of polyaniline.

2. Experimental

2.1. Reactants

Aniline (reagent grade) and H_2SO_4 (suprapure) were supplied by Merck. Aniline was distilled before use. The ultrapure water (18.2 $M\Omega$ cm) was obtained from a Millipore-MilliQ system. D_2O (99.9%-D) was supplied by Aldrich.

2.2. Cyclic voltammetry

The working electrode was a platinum polycrystalline electrode (0.1 cm^2) and the counter electrode was a platinum wire. All potentials were measured against the reversible hydrogen electrode (RHE) immersed in the working solution through a Luggin capillary. The electrochemical measurements were performed by using a bipotentiostat-galvanostat (Pine instrument AFCBP1 model) equipped with an EDAQ e-corder 410.

2.3. Electropolymerization of aniline

The working electrode was thermally cleaned and subsequently protected from the laboratory atmosphere by a droplet of ultrapure (or deuterated) water. Then, it was transferred to the working solution (previously deaerated by bubbling N_2) where it was immersed at controlled potential (0.1 V). The electropolymerization of aniline was carried out in 0.1 M aniline + 0.5 M H_2SO_4 solution.

PANI nucleation was performed by a single first cycle up to 1.15 V. Then, 7 cycles were performed to an upper limit set at 1.05 V to avoid the degradation of the polymer during the growth (see fig. S1 in the supporting information).

2.4. In situ FTIR measurements

A mirror-polished working electrode (1 cm^2) was used in this case. The electrode was coated with a PANI deposit as thin as 100 nm to minimize the effect of light dispersion. After the electrochemical synthesis, the electrode was rinsed repeatedly with either ultrapure or deuterated water and transferred to a Nicolet Magna 850 spectrometer for the *in situ* FTIR experiments. The spectroelectrochemical cell was
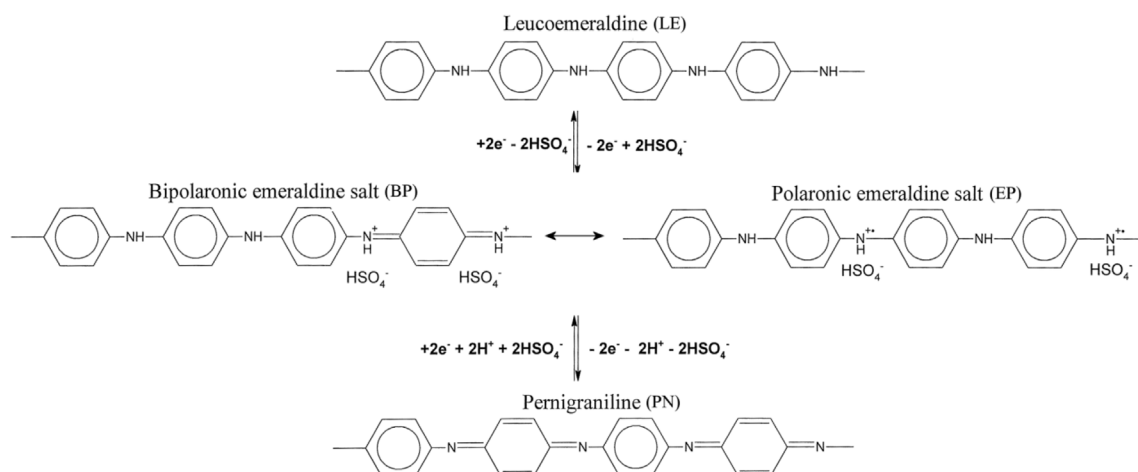
Scheme 1. Current tetrameric structure describing PANI transitions. The initial leucoemeraldine structure is presented in the base form for visual simplicity.

provided with a prismatic CaF$_2$ window beveled at 60° to work in the external reflection-absorption mode (FT-IRRAS) [40].

0.1 M H$_2$SO$_4$ in either H$_2$O or D$_2$O was employed as the supporting electrolyte. The final D/H ratio was about 500 in D$_2$O solutions. No monomer was added to the working solution. The electrode was immersed at 0.1 V and then cycled in the 0.1–0.7 V potential range to test the first reversible redox response, and, after this treatment, the potential was maintained at 0.1 V until equilibration. At this point, one of the following experimental procedures was applied.

a) A reference spectrum (100 interferograms) was acquired at 0.1 V (potential at which PANI is in its reduced form). The potential was then stepped sequentially in the positive direction and sets of 100 sample interferograms were collected for every step.

b) A reference spectrum was acquired at 0.1 V (2 interferograms). The potential was then swept in the positive direction at 1 mV/s and sets of 2 sample interferograms were collected simultaneously every 100 mV.

Finally, each sample spectrum (R) corresponding to a potential was referred to the reference spectrum collected previously (R$_0$ in the usual form (R-R$_0$)/R$_0$). In this way, the processed spectra will show positive (upwards) bands for IR modes present only (or largely) at the reference potential whereas negative bands (downwards) will reflect the creation of new active modes at the sample potential. All the spectra were collected at 8 cm^{-1} resolution using either *p*- or *s*-polarized radiation.

2.5. In situ conductance measurements

PANI was deposited electrochemically on top of an independently addressable 5-μm microband platinum electrode deposited on a substrate made of Borosilicate Glass (*ABTECH Scientific IAME 0504-Pt*, Platinum, 5 mm-long lines and with 5-μm band spacings). The electropolymerization was carried out by connecting all four probes to the same working contact and growing PANI potentiodynamically as indicated above. Film uniformity and integrity was assured for each individual Pt microband electrode by recording virtually identical cyclic voltammograms in 0.1 M H$_2$SO$_4$. Conductance measurements were performed in the same electrolyte solution by following a method similar to that presented by Nishizawa et al. [41]. The potential of a couple of electrodes (*W1* and *W2*) was scanned at 20 mV s^{-1} while maintaining an offset potential between them of ΔV(offset) = 5 mV (see Scheme 2). A potential difference was measured between the inner probe bands, *P1* and *P2*. The values of ohmic (i_R) and faradic currents (i_F) can be extracted from the total currents passing through *W1* and *W2* electrodes by:

$$i_F = \frac{(i_2 + i_1)}{2} \tag{1}$$

$$i_R = \frac{(i_2 - i_1)}{2} \tag{2}$$

Being i_1 and i_2 the currents passing through the electrodes *W1* and *W2*, respectively.

The conductance of the film was determined using Ohm's law (3) at each potential, *G*:

$$G = \frac{i_R}{\Delta V(P2 - P1)} \tag{3}$$

where $\Delta V(P2 - P1)$ stands for the potential difference measured between the inner probes with an independent, high impedance voltmeter.

3. Results

Fig. 1 shows the well-known cyclic voltammogram recorded for PANI in sulfuric acid medium. This voltammogram displays two redox waves centered at 0.45 V and 1.05 V. The peak appearing at less pos-
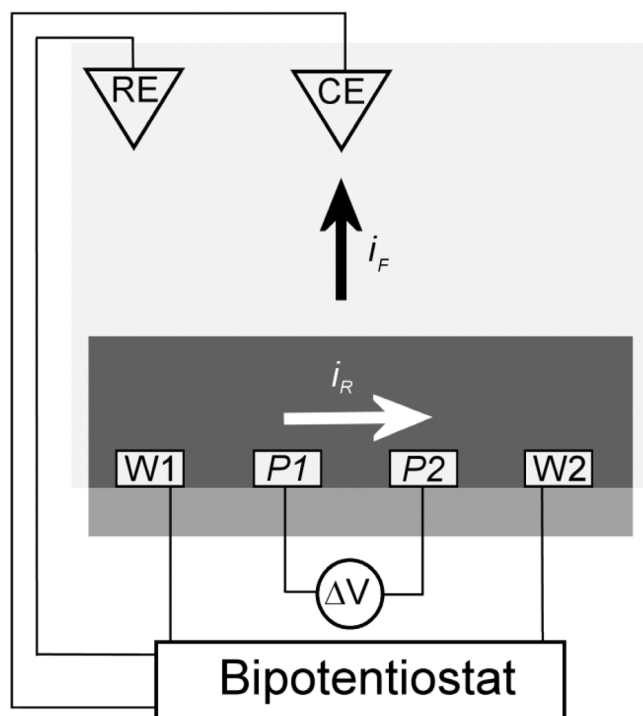
Scheme 2. Experimental setup for *in situ* conductance. RE is the reference electrode, CE is the counter or auxiliary electrode. W1 and W2 refer to outer working electrodes. *P1* and *P2* correspond to inner sensing electrodes.

itive potentials (I) is attributed to the reversible oxidation of PANI from the fully reduced form leucoemeraldine to emeraldine, the half-oxidized polymer. On the other hand, the second peak (II) has been assigned to the reversible redox transformation of emeraldine into pernigraniline. The intermediate peak appearing around 0.7 V (with very low intensity in the present case) is usually assigned to either
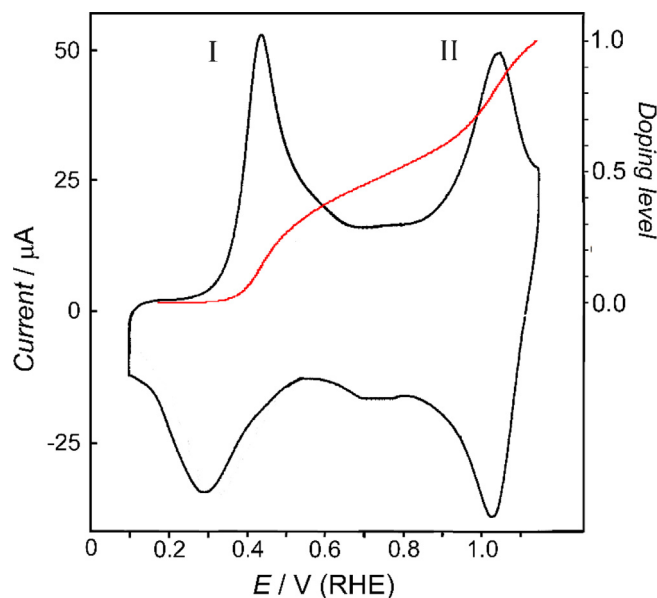

Fig. 1. Cyclic voltammograms recorded in 0.1 M H$_2$SO$_4$ for a PANI film and corresponding doping level at each potential (red curve, right axis). Scan rate 50 mV s^{-1}. (For interpretation of the references to colour in this figure legend, the reader is referred to the web version of this article.)

cross-linking between polymer chains [42] or to the appearance of diverse hydrolysis products [43,44].

The amount of charge injected into the polymer can be quantified by integration of the voltammetric curve in Fig. 1. A value of + 0.76 V (+0.56 V over the oxidation onset) was ascribed to a doping level of 0.5, under the assumption that the emeraldine state is attained at a potential corresponding to a charge averaging that passed up to the first and that passed up to the second transition peak. Similarly, the pernigraniline state (doping level 1) is reached at twice this value, which corresponds to a potential of + 1.12 V. Details on the calculation of the doping level can be found in the supporting information. The scale for doping level (i.e., electronic charge injected per monomer unit) derived from the integration of the voltammetric charge is included as the right axis in Fig. 1. The red curve represents the progress of doping level at increasing potential.

We have considered that the current involved after the doping peak corresponds to surface-confined faradic process in the polymer (pseudocapacitive current). Although voltammetric currents after the doping process (current *plateau*) occasionally present capacitive character, it seems more appropriate to take into consideration the molecularity of the system [45]. In this sense the oligomer approach, extensively discussed by Heinze, provides a comprehensive model for the electrochemical behaviour of conducting polymers [46]. Therefore, the plateau appearing in the voltammogram between 0.6 and 0.8 V in Fig. 1 is mainly due to the overlapped faradaic redox processes of chains with different conjugation lengths. The fact that the polymer is polydisperse favours this effect. In other words, the electrochemical charging process of conducting polymers is described by a sequence of discrete but overlapping redox faradic steps.

The doping process of PANI is linked to the formation of conductive species, free polarons, which are chemically described as radical entities bearing unpaired electrons. Free polarons can be detected by electron spin resonance (ESR) spectroscopy and visualized as semiquinone rings, as depicted in Scheme 3.

The formation of such species, representing a free charge carrier, stimulates sharp changes in conductivity upon electrochemical oxidation [47,48]. Fig. 2 shows *in situ* conductance measured during the electrochemical doping of PANI. Below 0.2 V the polymer is still in its reduced (leucoemeraldine) state and, accordingly, presents very low conductance. Interestingly, at potentials beyond the oxidation onset of the polymer, conductivity fluctuates according to four different regimes. At the early doping stages, (represented as segment I in Fig. 2b) conductance remains low, in the order of 10^{-6} S at 0.3 V (doping level 0.007), which means that free polaronic species can be neglected in this regime. Conductance increases then exponentially between 0.3 V and 0.4 V (doping level 0.007 to 0.07) with an observed slope close to 29 mV decade^{-1}, as seen in the supporting information, Fig. S3. This number is in the order of magnitude found for other electrochemically prepared conducting polymers, such as polypyrroles or polythiophenes [49,50].

From 0.4 V to 0.65 V (segment III, doping level 0.07 to 0.45) PANI conductance still progresses at increasing doping levels, but at a lower rate. The highest value recorded, 0.01 S, is almost four orders of magnitude larger than the initial value and is reached at 0.62 V (doping level 0.41). From this point, a small charge injection causes conductance to drop softly until the emeraldine redox state is completely reached (0.77 V, doping level 0.5). Finally, a sharp decrease is recorded in the potential region corresponding to the transition from
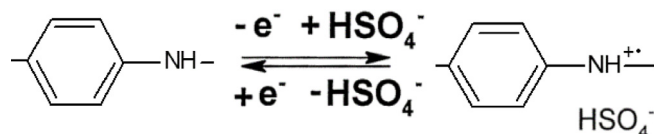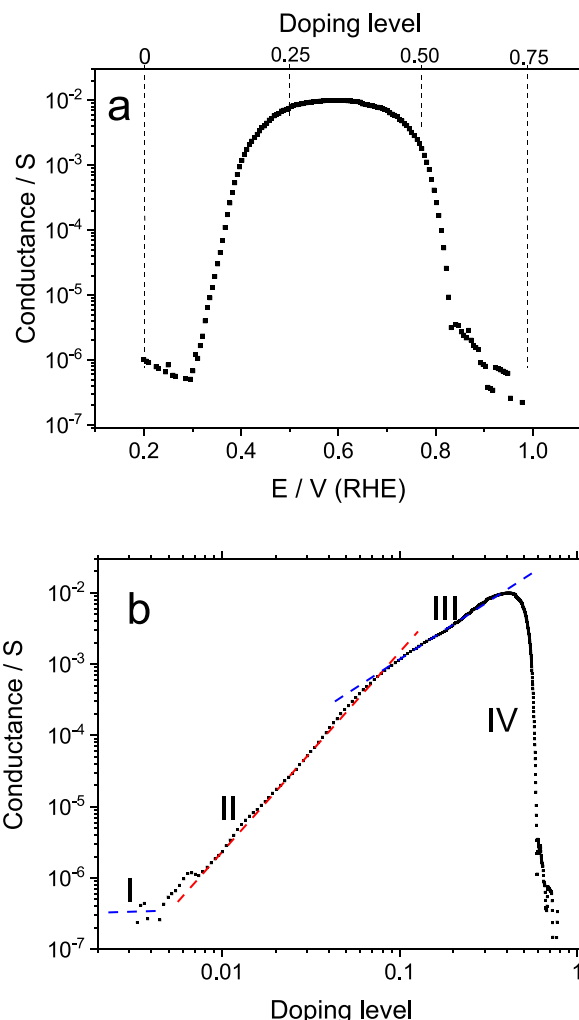

Fig. 2. Conductance measured *in situ* for a PANI thin film against (a) applied potential and (b) doping level.

emeraldine to pernigraniline state (segment IV). Conductance reaches eventually a value similar to that of the leucoemeraldine initial state.

It is widely accepted that electrochemical oxidation beyond the emeraldine redox state stimulates deprotonation of polymer chains, which is responsible for the lack of conductivity of the polymer when pernigraniline is formed. In this context, *in situ* FTIR spectroscopy can be used to monitor the effect of changing the potential on the chemical structure of the polymer. Fig. 3 shows *in situ* FTIR spectra collected in 0.1 M H_2SO_4/H_2O at 0.5 V, 1.0 V and 1.2 V sample potentials for a thin PANI film in the absence of aniline monomer. The reference spectrum was acquired firstly at 0.1 V, so it contains the vibrational information corresponding to the fully reduced form of the polymer. By referring each of the sample spectra to the single reference collected previously, the group of processed FTIR spectra was obtained.

As shown in Fig. 2, the onset of polymer doping occurs at around 0.3 V. The number of chemical changes involved at so low doping level should be very scarce. However, *in situ* FTIR reveals positive (upwards) and negative (downwards) features in the spectra collected at sample potentials higher than 0.2 V (see Fig. S4 in the Supporting Information). The intensity of such bands increases at higher potentials and they can be observed in Fig. 3 at 0.5 V (doping level 0.25), just above the first anodic maximum (peak I) on the cyclic voltammogram of Fig. l. The absorption at 1520 cm^{-1} is usually ascribed to the aromatic C—C ring-stretching vibration of benzenoid rings whereas the feature
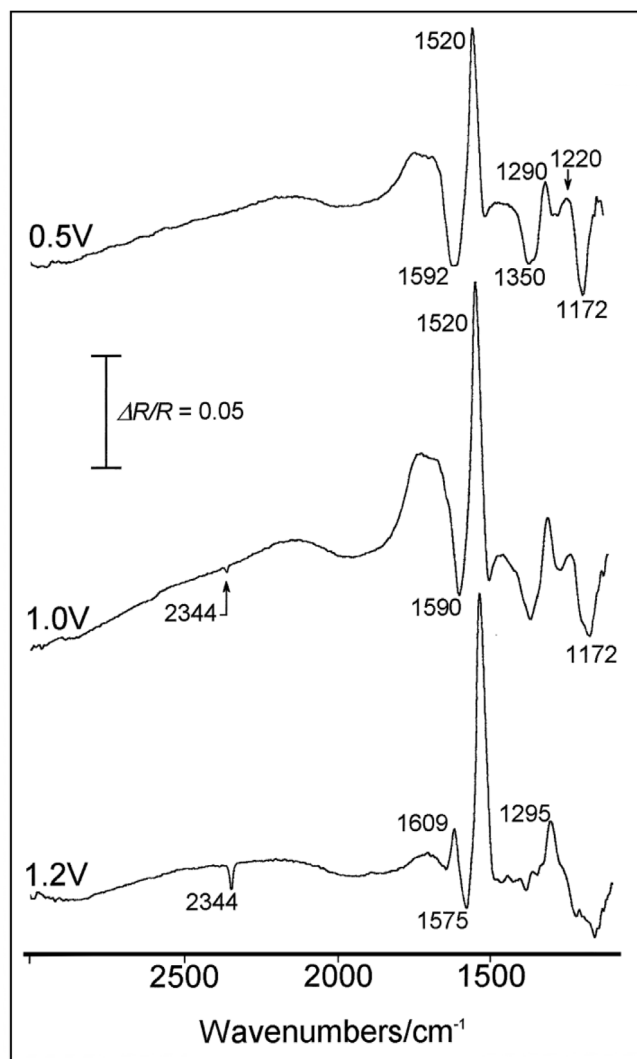

Scheme 3. Initial stage of leucoemeraldine oxidation.

Fig. 3. *In situ* FTIR spectra collected during the oxidation of an electrochemically synthesized PANI film in 0.1 M H_2SO_4/H_2O test solution. Reference potential 0.1 V. Sample potential labeled for each spectrum. 100 interferograms at each potential. *p*-polarized radiation.

at 1290 cm^{-1} is related to the aromatic ring deformation [25]. Their positive character reflects a decrease in the population of benzenoid structures due to PANI oxidation. In the same way, the positive-going band at 1220 cm^{-1} is ascribed to the disappearance of amine stretching modes of leucoemeraldine to yield imine-type bonds [18,25]. An additional negative-going broad band can be observed at 1592 cm^{-1}, which partially overlaps the uncompensated, strong absorption coming from H_2O bending in the same spectral region. This feature is connected with the C=C stretching of quinoid rings that are generated during oxidation [25,51]. Finally, this spectrum shows two negative-going bands of 1172 and 1350 cm^{-1}. The former is mostly attributed to in-plane C—H bending in quinoid structures [52] and the latter to a C—N stretching in semiquinoid units, although the marginal presence of this vibrational mode coming from phenazine-type rings cannot be ruled out [53,54]. At this point, it is worth noting that the semiquinoid C—N feature appears at a higher potential than the C=C stretching of quinoid rings (Fig. S4, Supporting Information).

The shape of the spectrum collected at 1.0 V (doping level 0.75) does not differ significantly from that recorded at 0.5 V. The intensification of the 1520 cm^{-1} band suggests further oxidation of reduced rings compared to 0.5 V. What seems significant in this spectrum is a very weak band at 2344 cm^{-1} that reveals the onset of carbon diox-

ide formation. This result points to the occurrence of degradation at potentials lower than those corresponding to peak II on the cyclic voltammogram, probably through the hydrolysis and mineralization of terminal defects, as quinone or quinone-imine, in some polymer chains [43]. The CO_2 absorption can be better perceived in the spectrum collected at 1.2 V (doping level >1), a potential at which PANI overoxidation is significant because is beyond the second oxidation maximum. It is also noticeable that this latter spectrum shows a strong alteration in the 1100–1500 cm^{-1} frequency which may reveal changes in the polymer structure due to overoxidation. For instance, the positive-going band peaking at 1609 cm^{-1} has been attributed in some studies to a disorder-induced C—C aromatic ring stretching mode [18].

The question that arises at this point is whether or not soluble products (apart from CO_2) are released from PANI by overoxidation at potentials around the second oxidation peak. Again, *in situ* FTIR spectroscopy can help in carrying out this task thanks to the use of *s*-polarized radiation. Usually, the polarization of the incident IR beam in a plane parallel to the electrode surface (*s*-polarized) provides a way to discriminate vibrational modes coming from species present in the bulk solution, a phenomenon known as the surface selection rule for electrochemical interfaces [40]. However, owing to the actual three-dimensional characteristics of a PANI deposit, *s*-polarized radiation is expected not to be fully insensitive to vibrational modes next to the electrode surface. To focus the study on soluble species, the combined use of *s*-polarized radiation and deuterated water as the solvent is preferable because spectral interferences coming from water bending in the surroundings of 1600 cm^{-1} are avoided. According to this premise, a set of spectra were collected for the PANI deposit at sample potentials around peak II in D_2O/H_2SO_4 and the results are shown in Fig. 4. The presence of a positive-going band at 1516 cm^{-1} reveals the vanishing of aromatic C—C vibrations at 1.0 V in PANI (the reference spectrum was acquired previously at 0.1 V). The activation of this vibrational mode under *s*-polarized radiation is associated, as mentioned above, with the three-dimensional character of the sample. Interestingly, the spectrum obtained at 1.1 V (at around the maximum of the voltammetric peak II) shows an additional clear-cut band centered at 1657 cm^{-1} whose frequency is characteristic of C=O stretching in soluble quinones [19,39]. The intensity of this feature increases significantly at 1.2 V, thus showing an enhanced degradation of PANI chains induced by the potential.

To facilitate a correlation between FTIR spectra and the CV profile during the gradual oxidation process undergone by PANI from its fully reduced state, the potential of a thin polymer film in contact with a sulfuric acid electrolyte in deuterated water as the solvent was swept from 0.1 up to 1.2 V, while sample spectra were collected simultaneously (see the experimental section for details). The results of this experiment are shown in Fig. 5, where the intense positive-going band at 1519 cm^{-1} (aromatic C—C stretching) reveals the disappearance of benzenoid rings and the less intense band at 1594 cm^{-1} is assigned to the formation of C=C as a result of polymer oxidation. In addition to these two main absorptions, the spectra in Fig. 5 show also an overlapping band at 1620 cm^{-1}, undetected in Fig. 3 because of H_2O absorption. Its position and negative character are both compatible with the presence of C=N vibrational modes in quinone-imine structures [18,55], but it may also include a contribution from C=C stretching vibration in phenazine-like segments [53].

Band intensities coming from C—C and C=C vibrations are integrated as a function of the applied potential in Fig. 6. The integration of the latter was carried out between 1573 cm^{-1} and 1598 cm^{-1} to minimize interference from the overlapped C=N stretching.

The vanishing of the aromatic C—C stretching mode (red squares) rises sharply at low oxidation potentials and starts leveling off at a potential close to 0.6 V, which corresponds to a doping level of 0.4 in Fig. 1. Above 0.6 V the loss of benzenoid rings is negligible (less than 6%) when compared to the drop that occurred between 0.3 V
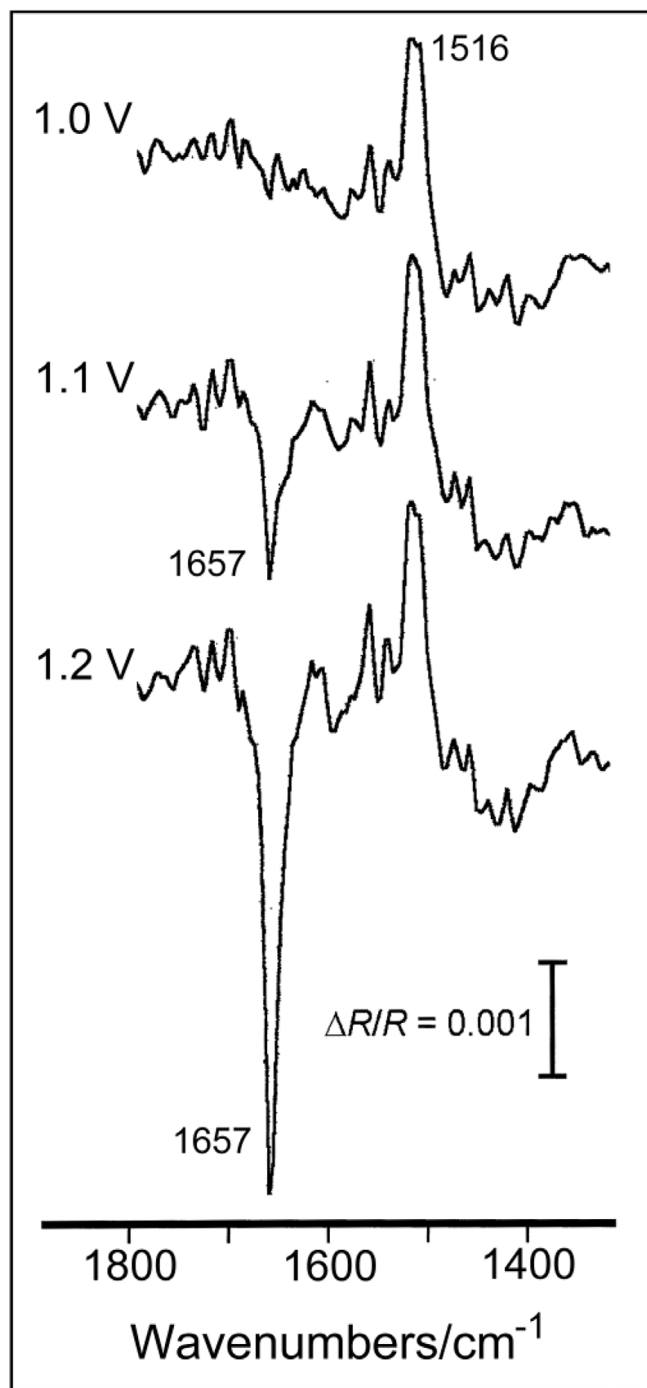
Fig. 4. FTIR analysis of soluble species released from PANI in 0.1 M H_2SO_4/D_2O. Sample potentials are indicated for each spectrum. The reference potential is 0.1 V in all cases. 100 interferograms were collected at each potential. *s*-polarized radiation.

Fig. 5. Set of *in situ* FTIR spectra collected for PANI during a potential scan up to 1.2 V. Test solution 0.1 M H_2SO_4/D_2O. Reference potential 0.1 V. Sample potential labeled for each spectrum. 2 interferograms at each potential. *p*-polarized radiation.

and 0.6 V. On the contrary, the population of C=C (black squares in Fig. 6) seems to grow during the first stages of PANI oxidation, then passes through a maximum at a potential close to 0.5 V (which represents a doping level of 0.25) and decreases to a minimum at 0.7 V (doping level at around 0.45). Further oxidation results in an additional growth peaking at 1.0 V (doping level 0.75) and a final decline of the vibrational mode.

The redox transformations of this polymer are often described based on the tetrameric structures shown in Scheme 1, which explain
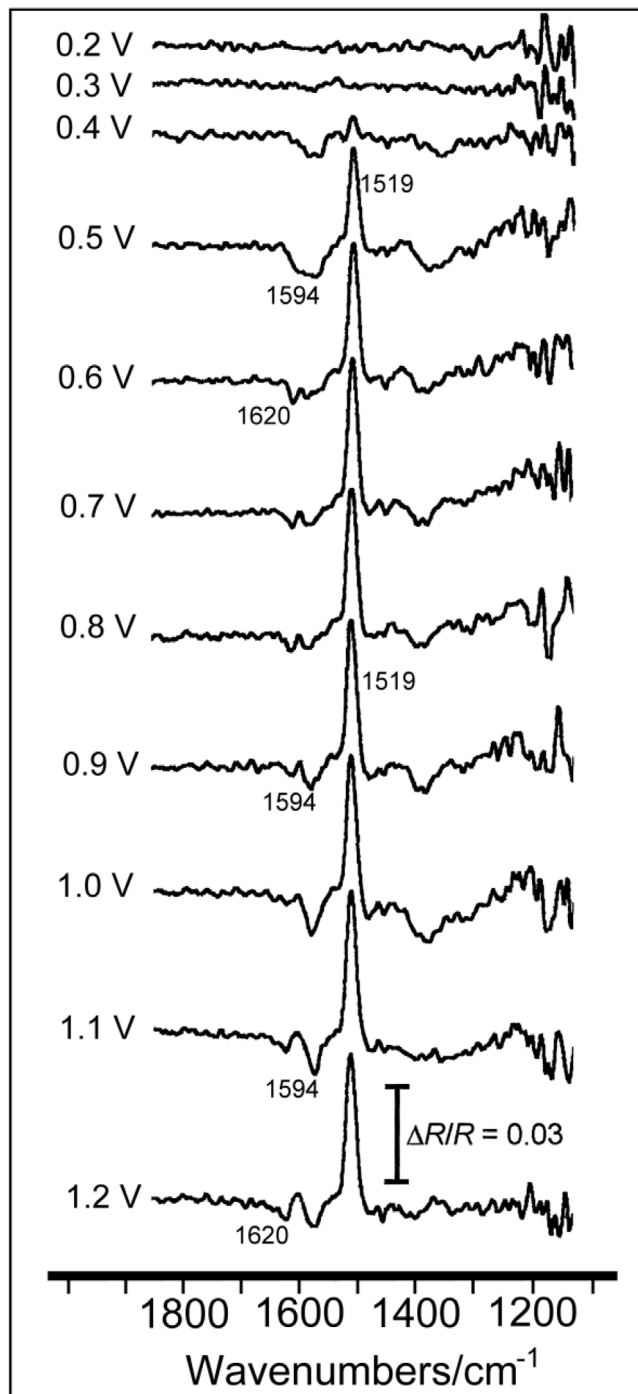
the chemical processes involved. Leucoemeraldine is accepted to be formed exclusively by benzenoid rings, the emeraldine form presents 1 quinoid ring per 3 benzenoid rings and pernigraniline contains 1 quinoid per benzenoid ring. According to this idealized picture, one should expect the aromatic C—C band to exhibit half the maximum recorded intensity loss at the 0.5 doping level state (at about 0.75 V) and then change by the remaining 50% to reach its highest loss at the positive end of the CV, where all the polymer should be in the fully oxidized pernigraniline state. However, the tetrameric model predic-
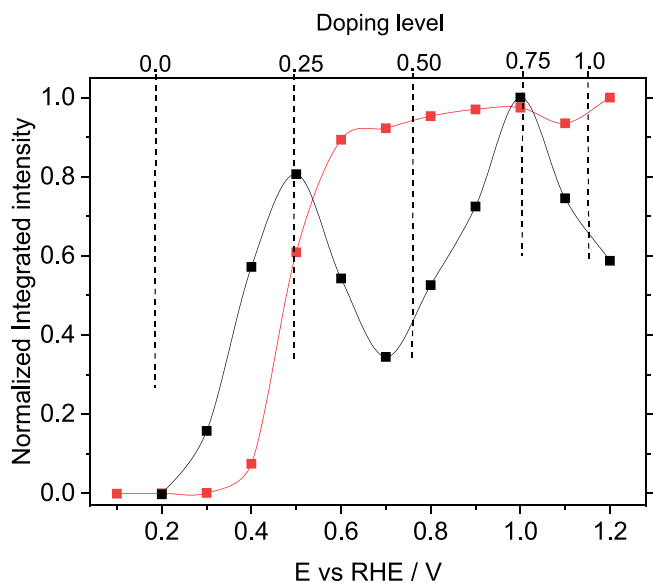
Fig. 6. Potential dependence of the normalized integrated band intensity from PANI aromatic C—C stretching (■) and quinoid C=C stretching (■). Data obtained from Fig. 5. The doping level of the polymer at selected potentials is also included.

tions do not match the experimental findings reported in this work. Our results suggest that the voltammetric charge recorded between 0.7 V and the maximum of the anodic peak (II) is not consumed in the transformation of a significant number of benzenoid rings, but it is certainly related to an increase in the population of quinoid rings. Above peak (II), where pernigraniline is the expected redox state, the amount of quinoid structures diminishes whereas the population of benzenoid rings keeps nearly constant. It can be then concluded that the semi-quantitative results obtained by FTIR are difficult to fit within the current PANI tetrameric model.

4. Discussion

To make a proper quantification of the *in situ* FTIR signals appearing during the redox transitions of the polymer, 4 different species should be considered according to the intensity of the corresponding absorption. First, a benzenoid ring in its unoxidized state, which is bonded to secondary nitrogen. For this species, the nitrogen atom shows sp^3 hybridization and, consequently, bears a non-bonding orbital with paired electrons. This type of ring presents a strong IR signal ascribed to the aromatic C—C stretching mode. The conversion of benzenoid into semiquinone species obliges nitrogen to adopt sp^2 hybridization and, consequently, to leave a half-filled p_z orbital. This latter orbital can easily interact with π electrons of the adjacent aromatic ring disturbing aromaticity, as shown in Scheme 4, and therefore the IR signal coming from the aromatic C—C stretching mode in semi-quinones is very weak.

Deeper oxidation of the ring yields a quinoid species bonded to imine nitrogen that can be either protonated (as in emeraldine) or unprotonated (as in pernigraniline). In this case, the term protonation refers to changes in the protonation level of the rings involved in the redox transition (not to the absolute protonation of the material). For example, leucoemeraldine is presented in base form (for visual clarity) but it is worth noting that part of the amine nitrogens in this material should be protonated [56,57].

As detected by *in situ* FTIR, the absorption intensity of the quinoid C=C stretching mode seems strongly influenced by its chemical environment. This effect was already reported [58] and ascribed to the release of a proton upon oxidation, which probably increases the sym-

metry of the absorbing center thus affecting absorptivity. Similar behavior was described in [23], where a noticeable intensity loss of the vibrational modes associated with oxidized units was observed upon deprotonation of emeraldine salt. As a result, the IR signal for the unprotonated quinoid ring weakens. In Table 1, the four-ring structures that can be present in PANI at different oxidation states are represented.

As discussed in Fig. 2, the presence of free polaron species (semiquinone in Table 1) was not detected below 0.3 V by conductivity measurements. This result agrees with the *in situ* FTIR spectrum shown in Fig. 2S (SI), for which the band assigned to protonated quinoid species (~1580 cm^{-1}) appears at potentials lower than those corresponding to the C—N stretching in semiquinoid units (~1330 cm^{-1}). These findings do not necessarily preclude the formation of radical cation species at doping levels below 0.004 e/monomer. They may occur as "isolated polarons" (in connection with the increase of the 430-nm optical absorption [28]) at too low a concentration to be discerned by our FTIR measurements. Interestingly, recent differential Raman spectra of polyaniline films subjected to low anodic potentials in acidic media showed no bands lying within 1320–1340 cm^{-1} (polaron C—N vibrations), even at laser excitation wavelengths giving rise to resonant enhancement of spectral features related to the oxidized forms of the polymer [59]. However, our experimental evidence suggest that the formation of protonated quinone-imine is favoured at doping levels below 0.004. In any case, neither protonated quinone-imine nor isolated radical cations provide significant conductivity to the polymer at this stage. According to this interpretation, the main redox transition occurring at the early stages of doping is represented in Scheme 5.

Within the 0.3–0.4 V potential window, which corresponds to doping values ranging between 0.004 and 0.1, there is a significant vanishing of aromatic vibrational modes and a concomitant growth of nearly 4 orders of magnitude in conductance. FTIR band intensity quantification suggests that each protoemeraldine octamer, the prevalent redox state at 0.5 V (doping level ~0.25), contains one protonated quinone-imine moiety (colored in orange), two protonated amine rings (blue) and five unprotonated aromatic rings (white). Such an arrangement is in essence similar to the bottom structure in Scheme 5. The sharp conductivity growth throughout this doping regime, together with the development of the C—N stretching in semiquinoid units, reveal the progressive formation of a resonant, electron-conducting protoemeraldine structure containing semiquinone rings.

In Fig. 6, the FTIR features of the protoemeraldine-emeraldine conversion between 0.5 and 0.7 V reveal an additional vanishing of benzenoid (white) rings in parallel to a decrease in the population of quinoneimines (orange). This result along with the measured increase in conductance, which reaches its maximum value at 0.6 V (doping level 0.4), strongly suggests the formation of two emeraldine resonant forms for which semiquinone (blue) rings are prevalent, as depicted in Scheme 6. In terms of the current tetrameric structure (Scheme 1) the resonance hybrid would be interpreted as having a proportion of 25% in bipolaronic and 75% in semiquinone moieties at different polymer chains.
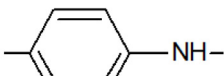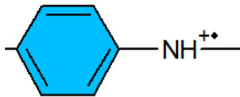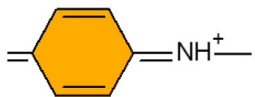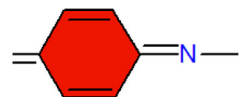
The upper structure in Scheme 6 was already proposed by Lux to model the conductivity of solid-state PANI [20] and implies the coexistence of bipolaronic and polaronic centers in the same chain. From the *in situ* FTIR standpoint, since only 3 or 4 white rings remain, bipolaronic and semiquinoid structures could both explain a maximum intensity decay of the aromatic C—C absorption at 0.8 V. However, the decrease of the quinoid band intensity to, roughly, half of its maximum value at around this potential (see Fig. 6) implies that the resonance hybrid is the most suitable description of the emeraldine redox state.

According to Fig. 6, as the oxidation proceeds above 0.8 V, the number of unprotonated aromatic rings remains constant but quinoid structures are progressively recovered. As a result, the conjugation length is shortened and hence conductance deteriorates during the
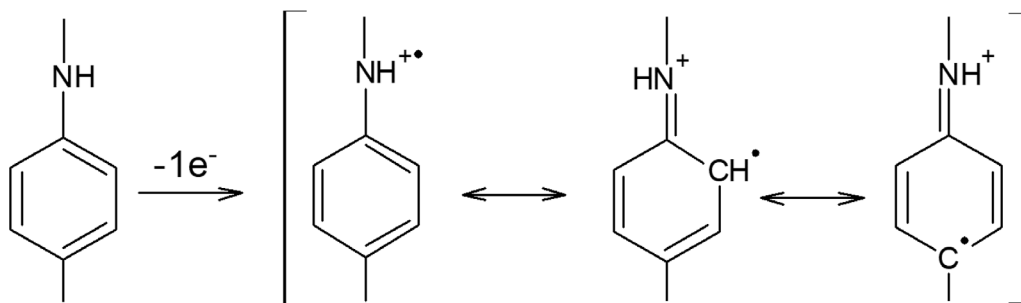
Scheme 4. First oxidation step of polyaniline.

Table 1
Ring structures present in PANI and observed intensity of the IR absorption.

Strong IR signal	Weak IR signal
Benzenoid	Semiquinone
Protonated quinoid	Unprotonated quinoid
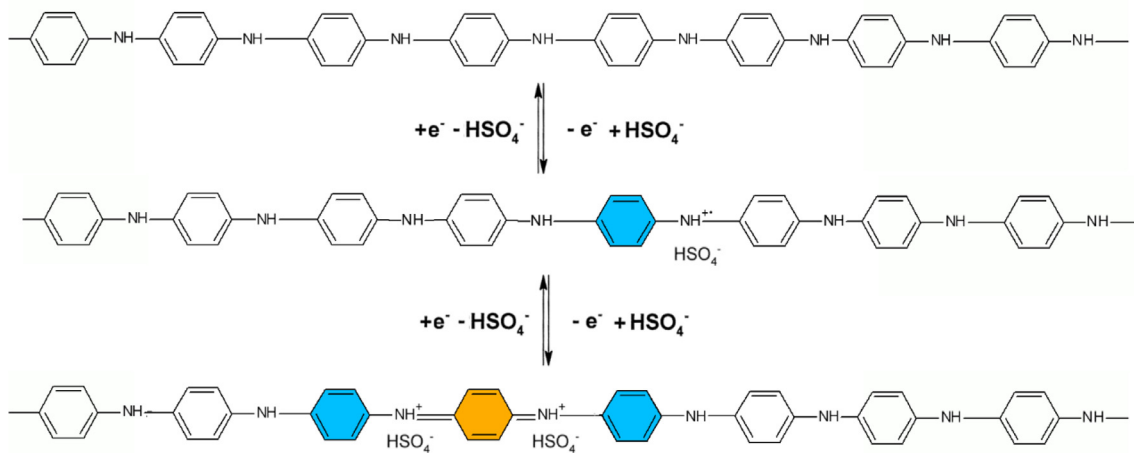
Scheme 5. Redox transition of PANI at doping level < 0.25. The leucomeraldine structure is represented in the base form for the sake of visual simplicity.
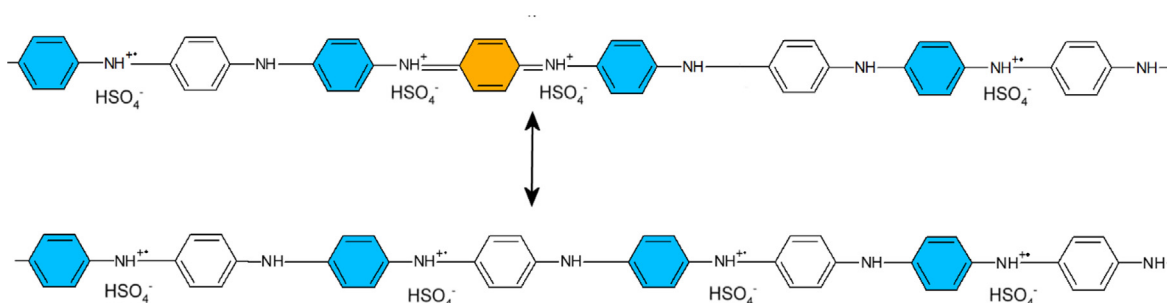
Scheme 6. Resonant forms of the emeraldine state at 0.76 V (doping level 0.50).
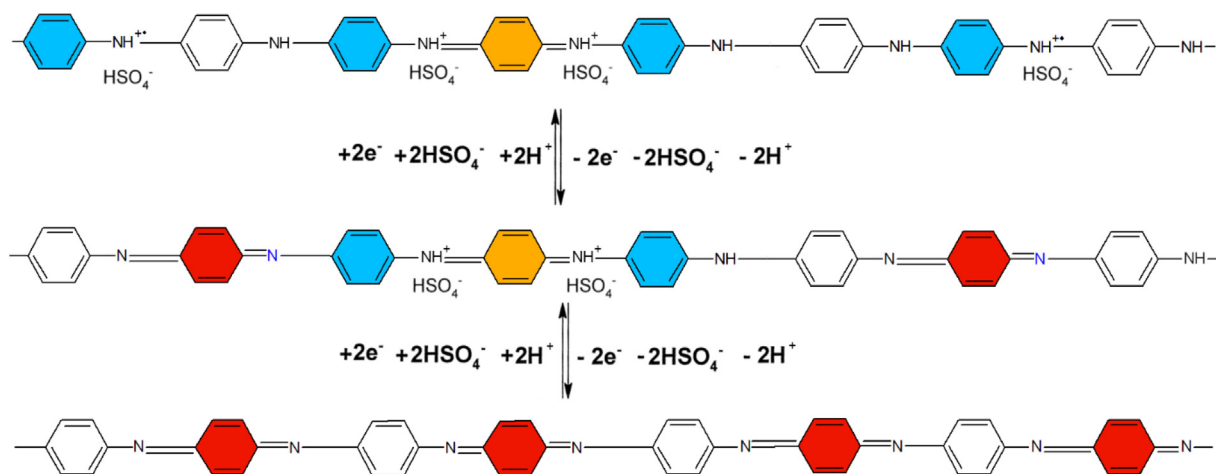
Scheme 7. Emeraldine to nigraniline (E >0.7 V) and nigraniline to pernigraniline redox transition (E >1.0 V).

emeraldine-nigraniline transformation (see Fig. 2). The polymer finally reaches the nigraniline redox state at a doping level of 0.75, which occurs in the surroundings of 1.0 V. This process is illustrated in the first step of Scheme 7, where no separate polarons are represented for nigraniline because the high concentration of charges favors the formation of unprotonated bipolaronic species (red rings) which, as deduced from Fig. 6, show weak infrared adsorption. Further oxidation beyond 1.0 V leads to the formation of the unprotonated, insulating form of PANI, pernigraniline [24]. As deduced from the spectra in Fig. 3, this redox transition is accompanied by the rupture of some polymer chains yielding soluble quinones and carbon dioxide.

As mentioned above, the overall redox response of PANI is currently described based on a tetrameric model. However, a better correlation between C—C vibrational modes and ring structures at different redox states can be found from the octameric model proposed in Schemes 5-7. This correlation, which relies on the quality of the molecular structure of synthesized PANI, will be more representative for long, linear polymeric chains and is not appropriate for describing the redox behavior of this material in crosslinking or overoxidized regions, among other chemical defects. The complete representation of PANI redox transitions can be found in Fig. 7, which also includes scales for doping level and applied potential.
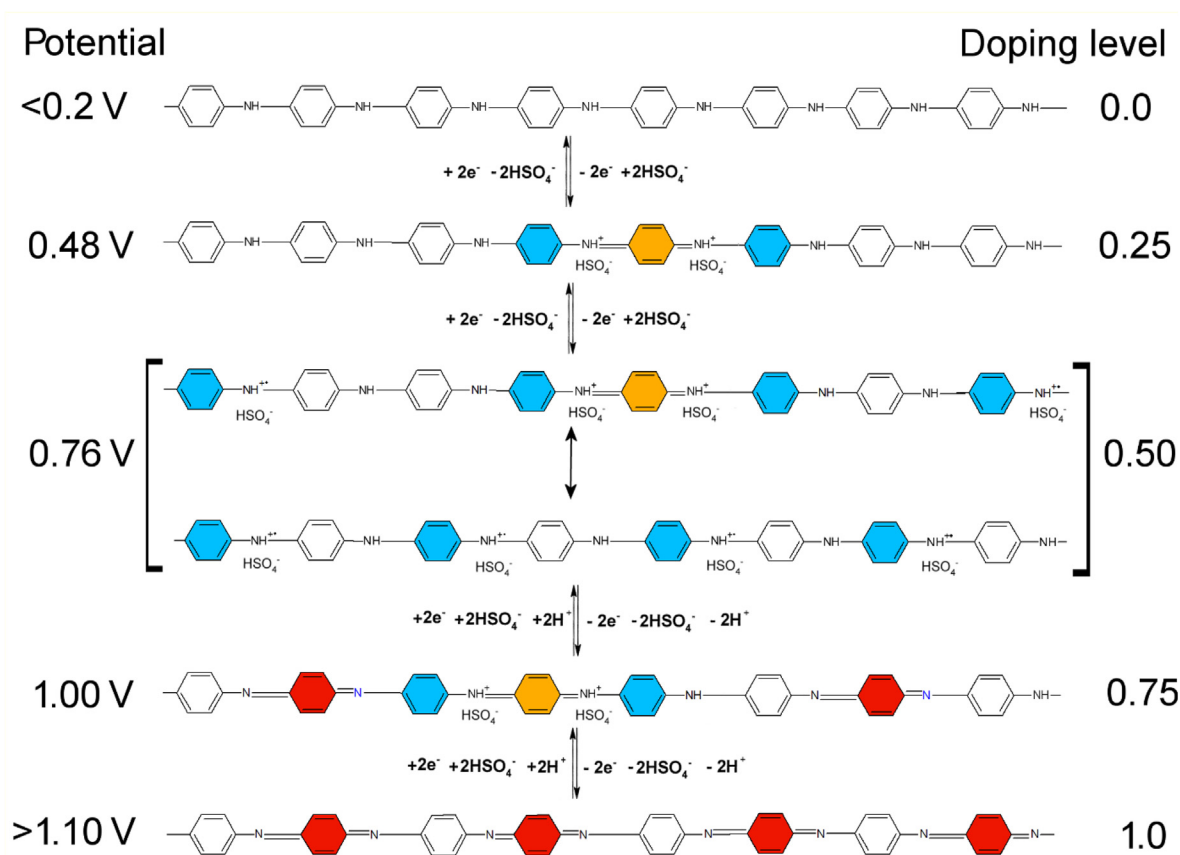

Fig. 7. Comprehensive model proposed for the redox transformations of PANI. This model summarizes the predominant chemical structures of a PANI octamer at different doping levels.

Based on that figure and according to the usual form of representing PANI redox states, the contribution of each particular ring structure to the corresponding redox state has been summarized in Table 2. Fractional numbers account for the partial contribution of resonance hybrids to each redox state.

The octameric model succeeds also in describing the relative intensity changes of IR absorptions during the potential excursion from the leucoemeraldine undoped state to the pernigraniline form. In Table 3, the experimental IR band intensities obtained from Fig. 6 for aromatic C—C and quinoid C═C stretching vibrations are collected. If a comparison is made with the intensity predicted from the octameric model, a good correlation is found, with the only discrepancy occurring for the nigraniline to pernigraniline transition.

Although the prediction qualitatively agrees with the observed decrease in both purely aromatic and protonated quinone-imine band intensities, the number of aromatic rings detected is lower than expected (a drop from 1 to 0.96 instead of 0.80) while the amount of protonated quinone-imine rings is higher than that suggested by the model (0.63). The sharp conductivity loss caused by deprotonation of emeraldine to yield pernigraniline (segment IV in Fig. 2) seems to be at the origin of these divergences. During this process, small, conducting domains of the polymer may become electrically isolated by broader insulating areas that most likely prevent them from reaching full oxidation to the pernigraniline state. The fast undoping process causes similar effects to other conducting polymers, giving rise to ion trapping phenomena, [60,61], where associated dopant anions/protons remain surrounded by an insulating matrix and are electrically retained within the polymer instead of being released. In the present case, the survival of small conducting domains embedded in a deprotonated pernigraniline dielectric structure would give rise to a recovery of purely aromatic structures lower than expected during the nigraniline to pernigraniline transition. The same argument applies to explain the unexpected prevalence of protonated quinone-imine units in the pernigraniline state. Furthermore, another effect that may cause a deviation from model predictions arises from the potential-induced degradation suffered by the polymer above 1.0 V (Figs. 3 and 4) which probably disturbs the accurate quantification of species by FTIR at so high potential.

5. Conclusions

Cyclic voltammetry, *in situ* conductance and *in situ* FTIR spectroscopy measurements were combined to gain deeper insight on the redox transitions of PANI in acidic medium. A return from the current 4-ring structure of PANI to the classical octameric model has been proposed to rationalize the results of the semiquantitative spectroscopic analysis.

In situ FTIR spectra of PANI are dominated by the aromatic C—C stretching (at around 1520 cm^{-1}) and the quinoid C═C stretching (1590 cm^{-1}) vibrations, whose intensity is found to be strongly influenced by the protonation level of the adjacent nitrogen atoms. In this way, PANI redox transitions stimulate changes in both C—C absorptions as they are associated with deep changes in the acidity of amine/imine bonds. It is suggested that the intensity of the aromatic C—C stretching located at radical cations weakens as a consequence of the change in nitrogen hybridization from sp^3 to sp^2. According to the semiquantitative redox model proposed, the population of aromatic rings reaches a minimum at the onset of emeraldine state and therefore these species are no longer (quantitatively) involved in subsequent redox transitions.

The emeraldine state is better described as a resonance hybrid of the classical bipolaronic and the semiquinoid (polaron lattice) structures. The observation that the population of protonated quinone-imine rings fluctuates at increasing potentials is interpreted in terms of the compromise reached between injected charge and resonant structures. Understanding these processes seems essential to make a suitable correlation between IR spectra, conductance, chemical structure and applied potential.

Finally, it is confirmed that most of the charge transferred at the onset of the second voltammetric peak comes from the additional oxidation of the resonance hybrid, which becomes unstable in the electrochemical environment producing mineralization to CO_2 and release of soluble quinones. According to this, pernigraniline should contain a significant amount of broken polymer chains with lower conjugation length, a picture that is supported by *in situ* conductance measurements. The most conducting form of PANI is obtained at a doping level close to 0.4, slightly below the actual emeraldine redox state.

CRediT authorship contribution statement

F. Huerta: Conceptualization, Investigation, Methodology, Formal analysis, Visualization, Writing - original draft, Writing - review & editing. **C. Quijada:** Validation, Formal analysis, Visualization, Writing - review & editing. **F. Montilla:** Methodology, Investigation, Formal analysis, Visualization, Writing - original draft, Writing - review & editing. **E. Morallón:** Funding acquisition, Supervision, Visualization, Writing - review & editing.

Table 2
Chemical speciation of PANI rings according to the octameric model.

	Strong IR absorption		Weak IR absorption	
	Purely aromatic	Protonated quinone-imine	Semiquinone	Unprotonated quinone-imine
Leucoemeraldine	8	0	0	0
Protoemeraldine	5	1	2	0
Emeraldine	3.5	0.5	4	0
Nigraniline	3	1	2	2
Pernigraniline	4	0	0	4

Table 3
Relative IR band intensity predicted by the octameric model and experimental values.

	Purely aromatic (white)		Protonated quinone-imine (orange)	
	Predicted	Experimental	Predicted	Experimental
Leucoemeraldine	0	0	0	0
Protoemeraldine	0.60	0.58	1.00	0.80
Emeraldine	0.90	0.94	0.50	0.43
Nigraniline	1.00	1.00	1.00	1.00
Pernigraniline	0.80	0.96	0	0.63

Declaration of Competing Interest

The authors declare that they have no known competing financial interests or personal relationships that could have appeared to influence the work reported in this paper.

Acknowledgments

Appendix A. Supplementary data

Supplementary data to this article can be found online at https://doi.org/10.1016/j.jelechem.2021.115593.

References

[1] S.R. Forrest, M.E. Thompson, Chem. Rev. 107 (2007) 923–925.
[2] G. Inzelt, Conducting Polymers A New Era in Electrochemistry, 2nd ed., Springer, 2015.
[3] T. Fernandez Otero, Conducting Polymers: Bioinspired Intelligent Materials and Devices, Royal Society of Chemistry, Cambridge, 2015.
[4] P. Audebert, F. Miomandre, in: Handb. Conjug. Polym, 4th ed., CRC PRESS-TAYLOR & FRANCIS GROUP, 2019, pp. 161–199.
[5] M. Romero, M.A. del Valle, R. del Río, F.R. Díaz, F. Armijo, E.A. Dalchiele, J. Electrochem. Soc. 160 (2013) G125–G134.
[6] G. Ciric-Marjanovic, Synth. Met. 177 (2013) 1–47.
[7] W.A. Marmisolle, D. Posadas, M.I. Florit, Electrochim. Acta 109 (2013) 894–900.
[8] C. Chen, T. Xu, A. Chen, L. Lu, Y. Gao, J. Electrochem. Soc. 163 (2016) G159–G165.
[9] S.C. Rasmussen, An Int. J. Hist. Chem. Subst. 1 (2017) 99–109.
[10] J. Lightfoot, The Chemical History and Progress of Aniline Black, Lower House, Burnlay, Lancashire, 1871.
[11] R. Willstätter, C.W. Moore, Berichte Der Dtsch. Chem. Gesellschaft 40 (1907) 2665–2689.
[12] A.G. Green, A.E. Woodhead, J. Chem. Soc. Trans. 97 (1910) 2388–2403.
[13] A.G. Macdiarmid, J.-C. Chiang, W. Huang, B.D. Humphrey, N.L.D. Somasiri, Mol. Cryst. Liq. Cryst. 125 (1985) 309–318.
[14] W.-S.S. Huang, B.D. Humphrey, A.G. MacDiarmid, J. Chem. Soc. Faraday Trans. 1 Phys. Chem. Condens. Phases 82 (1986) 2385–2400.
[15] E.M. Genies, M. Lapkowski, J. Electroanal. Chem. 220 (1987) 67–82.
[16] J.C. Chiang, A.G. MacDiarmid, Synth. Met. 13 (1986) 193–205.
[17] Z. Ping, G.E. Nauer, H. Neugebauer, J. Theiner, A. Neckel, Electrochim. Acta 42 (1997) 1693–1700.
[18] Z. Ping, G.E. Nauer, H. Neugebauer, J. Theiner, J. Electroanal. Chem. 420 (1997) 301–306.
[19] N.S. Sariciftci, H. Kuzmany, H. Neugebauer, A. Neckel, J. Chem. Phys. 92 (1990) 4530–4539.
[20] F. Lux, Polymer (Guildf). 35 (1994) 2915–2936.
[21] W.W. Focke, G.E. Wnek, J. Electroanal. Chem. 256 (1988) 343–352.
[22] J.Y. Shimano, A.G. MacDiarmid, Synth. Met. 123 (2001) 251–262.
[23] Z. Ping, J. Chem. Soc. – Faraday Trans. 92 (1996) 3063–3067.
[24] C.A. Barbero, Phys. Chem. Chem. Phys. 7 (2005) 1885–1899.
[25] G. Louarn, M. Lapkowski, S. Quillard, A. Pron, J.P. Buisson, S. Lefrant, J. Phys. Chem. 100 (1996) 6998–7006.
[26] J. López-Palacios, E. Muñoz, M.A. Heras, Á. Colina, V. Ruiz, Electrochim. Acta 52 (2006) 234–239.
[27] A. Neudeck, A. Petr, L. Dunsch, J. Phys. Chem. B 103 (1999) 912–919.
[28] A. Malinauskas, R. Holze, J. Appl. Polym. Sci. 73 (1999) 287–294.
[29] A. Abd-Elwahed, R. Holze, Synth. Met. 131 (2002) 61–70.
[30] E. Csahók, E. Vieil, G. Inzelt, J. Electroanal. Chem. 482 (2000) 168–177.
[31] E.M. Genies, P. Hany, M. Lapkowski, C. Santier, L. Olmedo, Synth. Met. 25 (1988) 29–37.
[32] P.S. Tóth, G.F. Samu, B. Endrodi, C. Visy, Electrochim. Acta 110 (2013) 446–451.
[33] G. Salinas, B.A. Frontana-Uribe, ChemElectroChem 6 (2019) 4105–4117.
[34] C. Barbero, J. Electrochem. Soc. 138 (1991) 669.
[35] A. Baba, S. Tian, F. Stefani, C. Xia, Z. Wang, R.C. Advincula, D. Johannsmann, W. Knoll, J. Electroanal. Chem. 562 (2004) 95–103.
[36] M. Trchová, I. Šeděnková, J. Stejskal, Synth. Met. 154 (2005) 1–4.
[37] A. Kellenberger, E. Dmitrieva, L. Dunsch, J. Phys. Chem. B 116 (2012) 4377–4385.
[38] R. Yan, B. Jin, J. Electroanal. Chem. 743 (2015) 60–67.
[39] G.A. Planes, J.L. Rodríguez, M.C. Miras, G. García, E. Pastor, C.A. Barbero, Phys. Chem. Chem. Phys. 12 (2010) 10584–10593.
[40] T. Iwasita, F.C. Nart, Prog. Surf. Sci. 55 (1997) 271–340.
[41] M. Nishizawa, T. Ise, H. Koshika, T. Itoh, I. Uchida, Chem. Mater. 12 (2000) 1367–1371.
[42] E.M. Geniès, M. Lapkowski, J.F. Penneau, J. Electroanal. Chem. 249 (1988) 97–107.
[43] Y.-B. Shim, Mi-Sook Won, Su-Moon Park, J. Electrochem. Soc. 137 (1990) 538.
[44] L. Duić, Z. Mandić, S. Kovač, Electrochim. Acta 40 (1995) 1681–1688.
[45] T.F. Otero, I. Boyano, M.T. Cortes, G. Vazquez, Electrochim. Acta 49 (2004) 3719–3726.
[46] J. Heinze, B.a. Frontana-Uribe, S. Ludwigs, Chem. Rev. 110 (2010) 4724–4771.
[47] J. Lippe, R. Holze, Synth. Met. 43 (1991) 2927–2930.
[48] D. Wei, A. Petr, C. Kvarnström, L. Dunsch, A. Ivaska, J. Phys. Chem. C 111 (2007) 16571–16576.
[49] H. Mao, P.G. Pickup, J. Am. Chem. Soc. 112 (1990) 1776–1782.
[50] J. Ochmanska, P.G. Pickup, J. Electroanal. Chem. 297 (1991) 211–224.
[51] Z. Ping, H. Neugebauer, A. Neckel, Electrochim. Acta 41 (1996) 767–772.
[52] M. Cotarelo, F. Huerta, C. Quijada, F. Cases, J. Vázquez, Synth. Met. 144 (2004) 207–211.
[53] M. Trchová, Jaroslav Stejskal, Pure Appl. Chem. 83 (2011) 1803–1817.
[54] M.A.A. Cotarelo, F. Huerta, C. Quijada, R. Mallavia, J.L.L. Vázquez, J. Electrochem. Soc. 153 (2006) D114.
[55] M. Abidi, S. López-Bernabeu, F. Huerta, F. Montilla, S. Besbes-Hentati, E. Morallón, Eur. Polym. J. 91 (2017) 386–395.
[56] W.A. Marmisollé, M.I. Florit, D. Posadas, J. Electroanal. Chem. 734 (2014) 10–17.
[57] D.W. Hatchett, M. Josowicz, J. Janata, J. Phys. Chem. B 103 (1999) 10992–10998.
[58] N. Chandrakanthi, M.A. Careem, Polym. Bull. 45 (2000) 113–120.
[59] R. Mažeikienė, G. Niaura, A. Malinauskas, Spectrochim. Acta – Part A Mol Biomol. Spectrosc. 221 (2019) 117147.
[60] J. Arias-Pardilla, T.F. Otero, R. Blanco, J.L. Segura, Electrochim. Acta 55 (2010) 1535–1542.
[61] A.R. Hillman, S.J. Daisley, S. Bruckenstein, Electrochim. Acta 53 (2008) 3763–3771.